THE ELECTROMECHANICAL IMPEDANCE SPECTROSCOPY METHOD ON THIN PLATES AT INTERMEDIATE AND HIGH FREQUENCIES

CRISTIAN RUGINA , VETURIA CHIROIU, LIGIA MUNTEANU

Abstract. This paper present a study of the electro-mechanical impedance spectroscopy method (EMIS) used in structural health monitoring with piezoelectric wafer active sensors, with and without wire lead connections, bonded on thin plates, at intermediate and high frequencies. For simple geometries like circular piezoelectric wafer active sensor bonded to circular plates, a simplified 2D axisymmetric analytic model exist, and is briefly presented. However when cracks exist the 2D model could not be applied. Usually the low frequencies (10kHz–150kHz) are used in the EMIS method. A 3D finite element method is used to analyze ability of the EMIS method to evaluate the distance to the crack at intermediate (150kHz–300kHz) and high (300kHz–450kHz) frequencies. The influence of the asymmetry position on the wire lead piezoelectric wafer active sensors related to the crack at intermediate and high frequencies is also studied. Quantifications by classical damage metrics are done.

Key words: electromechanical impedance spectroscopy method, EMIS, EMI, E/M, structural health monitoring, SHM, piezoelectric wafer active sensor, PWAS.

1. INTRODUCTION

The active and passive SHM systems become more and more used, especially on aerospace vehicles with thin plates structures [1, 11]. The active SHM sensing techniques are based on two different approaches: transient guided waves and standing waves [1]. In such SHM processes, a piezoelectric wafer active sensor (PWAS) is required to generate elastic waves. These travel along the mechanical structure, are reflected by different structural abnormalities, i.e., cracks, corrosions, delamination, and others, or from the boundary edges, and then are recaptured by the same sensor in a pulse–echo configuration or by other sensors of same or different type, even passive sensors, in pitch-catch configuration [1]; this is the so-called method of tuned Lamb waves. If the structural damage or boundary edges are in the close vicinity of the active sensor, their reflections overlap the incident

Institute of Solid Mechanics of the Romanian Academy, Bucharest

Ro. J. Techn. Sci. – Appl. Mechanics, Vol. 64, N° 2 P. 83–95, Bucharest, 2019

transient wave, making impossible the interpretation. This drawback can be overpassed by using the ultrasonic standing waves, in the so-called electromechanical impedance spectroscopy method (EMIS) (also known as EMI or E/M method). By sweeping the frequency of the input signals to PWAS, some changes appear in the impedance measured by an impedance analyzer connected to the PWAS terminals. By monitoring the changes in the real part of the impedance function, which is most sensitive to structural changes, one can evaluate the integrity of the host structure [1-4, 6, 7].

Usually the low frequencies (10kHz–150kHz), as defined in [1], are used. They give in the EMIS method relative big amplitude of the real part of the elecromechanical impdance. However at low frequencies [8] parasitic vibrations (acoustic and system vibrations) can induce subarmonics and supraarmonics which can interfere with the vibrations generated by the PWAS. So, a study of the EMIS method at intermediate (150kHz–300kHz) and high (300kHz–450kHz) frequencies is usefull.

The method is not only sensitive to structural changes, but also to geometrical imperfections, quality and thickness of the adhesive layer, properties of the piezoceramic material [3] and temperature [5, 9, 10]. The method is mainly experimental, but for simple geometries like circular PWAS bonded to circular plates, a simplified 2D axisymmetric analytic model exist and proven good at low frequencies [1, 2]. So this geometry is taken as a study base in this paper.

A numerical study based on a 2D axisymmetric finite element method (FEM), previously studied at low frequencies [3, 4], is done to compare the numerical results with analytic ones at intermediate and high frequencies.

Usually piezoelectric wafer active sensors with wire lead terminals (PWAS-WL) are used in SHM of non-metallic plates, or in SHM of metallic plates when an electric decoupling is needed [3]. So, a 3D FEM is also used in a sensitivity analysis of the influence of the asymmetry position of PWAS-WL with respect to the crack position involved in this SHM method at intermediate and high frequencies.

2. COMPUTATIONAL METHODS

2.1. The analytical method

For simple geometries like a circular PWAS bonded on the center of a circular plate, an analytical solution exists and an extended presentation is done in [1] and [2]. For a PWAS with radius r_a and thickness t_a, and a plate with radius a and thickness h (Fig. 1), the electrical impedance, as a function of the angular frequency of the excitation electrical signal, can be expressed [1-4]:

$$Z(\omega)=\left\{i\omega C\left[1-k_p^2+\frac{k_p^2}{2}\frac{(1+\nu_a)J_0(\varphi_a)}{\varphi_a J_0(\varphi_a)-(1-\nu_a)J_1(\varphi_a)-\chi(\omega)(1+\nu_a)J_1(\varphi_a)}\right]\right\}^{-1} \quad (1)$$

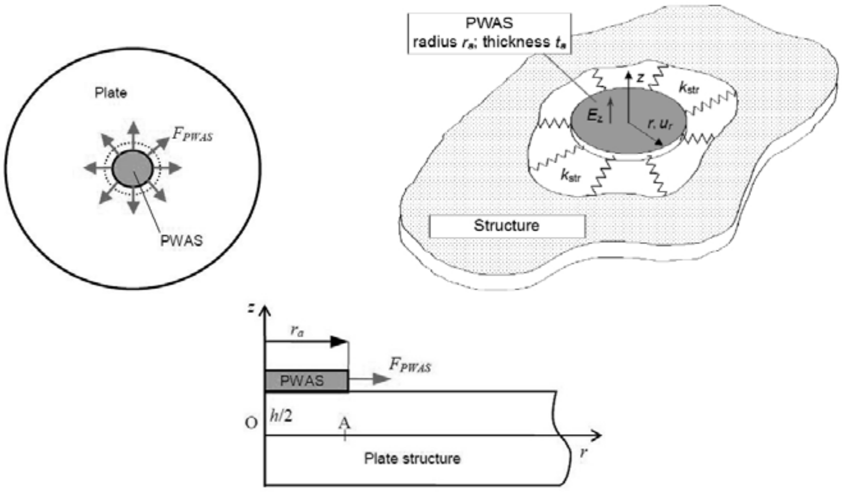

Fig. 1 – Circular PWAS constrained by structural stiffness, $k_{str}(\omega)$.

The coefficient k_p represents the planar coupling factor, given usually by the PWAS manufacturer, and expressed by:

$$k_p^2 = \frac{2d_{31}^2}{s_{11}^E(1-\nu_a)\varepsilon_{11}}. \tag{2}$$

The coefficient C represents the electrical capacitance of the PWAS, expressed by:

$$C = \frac{\varepsilon_{33}\pi r_a^2}{h}. \tag{3}$$

ν_a represents the Poisson ratio for PWAS, expressed by the ratio of the mechanical compliances coefficients s_{11}^E and s_{12}^E at zero electric field $(E=0)$:

$$\nu_a = -\frac{s_{12}^E}{s_{11}^E}. \tag{4}$$

$\varepsilon_{11}, \varepsilon_{33}$ represents the dielectric permittivity at zero mechanical stress $(T=0)$, and d_{31} represents the piezoelectric coupling between the electrical and mechanical variables.

The coefficient φ_a depends on the geometrical dimensions and the longitudinal wave speed c_P of the PWAS and is expressed by:

$$\varphi_a = \frac{\omega r_a}{c_P}, \quad c_P = \sqrt{\frac{1}{\rho s_{11}^E (1-\nu_a)}}. \tag{5}$$

Of course, when mechanical, piezoelectric and dielectric losses cannot be neglected complex values of those coefficients must be taken into account:

$$\bar{s}_{11} = s_{11}(1-i\eta), \quad \bar{\varepsilon}_{33} = s_{33}(1-i\delta), \quad \bar{C} = C(1-i\mu). \tag{6}$$

The coefficient $\bar{\chi}(\omega)$ in Eq.(1) represents the ratio of the mechanical stiffness of the structure to be monitored and the stiffness of the PWAS:

$$\bar{\chi}(\omega) = \frac{k_{str}(\omega)}{\bar{k}_{PWAS}}. \tag{7}$$

The stiffness of the PWAS, when the frequency spectrum taken into account in the SHM procedure is far from the PWAS resonances (radial, edge, thickness extensional and thickness shear) it can be expressed:

$$\bar{k}_{PWAS} = \frac{t_a}{r_a \bar{s}_{11}(1-\nu_a)}. \tag{8}$$

But the stiffness of the structure is different. The frequency spectrum of the excitation signal, is in the range of radial and flexural resonance of the structure. As shown in [1-4] it can be described, as the sum of two terms, the first one modelling the radial mode of vibration, while the second term is modeling the flexural mode of vibration of the circular plate with the bonded PWAS, and can be expressed:

$$k_{str}(\omega) = \rho a^2 \left[\frac{2}{h} \sum_k \frac{\left[r_a R_k(r_a) - \int_0^a R_k(r)\, H(r_a - r)\,\mathrm{d}r \right] R_k(r_a)}{-\omega^2 + 2i\zeta_k \omega\omega_k + \omega_k^2} + \right.$$
$$\left. + \frac{h}{2} \sum_m \frac{[3Y_m(r_a) + r_a Y_m'(r_a)] Y_m'(r_a)}{-\omega^2 + 2i\zeta_m \omega\omega_m + \omega_{j_w}^2} \right]^{-1}, \tag{9}$$

where H represents the Heaviside step function, while the mode shapes $R_k(r)$, for radial vibration mode, and $Y_m(r)$, for flexural vibration mode, expressed by:

$$R_k(r) = A_k J_0(\lambda_k r), \tag{10}$$

$$Y_m(r) = B_m \left[J_0(\lambda_m r) + C_m I_0(\lambda_m r) \right], \tag{11}$$

form an orthonormal function sets that satisfy the orthonormality conditions

$$\rho h\int_0^{2\pi}\int_0^a R_k(r)R_l(r)\,r\,\mathrm{d}r\,\mathrm{d}\theta=\rho\pi a^2 h\delta_{kl}\,, \tag{12}$$

$$\rho h\int_0^{2\pi}\int_0^a Y_p(r)Y_m(r)\,r\,\mathrm{d}r\,\mathrm{d}\theta=\rho\pi a^2 h\delta_{pm}\,. \tag{13}$$

For axial vibration of the plate, the coefficients λ_k from Eq. (10) are $\lambda_k = z_k / a$ where z_k are the solutions of the equation $z J_0(z)-(1-\nu)J_1(z)=0$ that describe the axial vibration of a circular plate in term of Bessel functions and Poisson ratio. The coefficients A_k in Eq. (10) are $A_k=\sqrt{J_1^2(z_k)-J_0(z_k)J_2(z_k)}$.

For flexural vibration of the plate, the coefficients λ_m from (11) are $\lambda_m = z_m / a$ where z_m is the solution of equation $\dfrac{\lambda^2 J_0(\lambda)+(1-\nu)\lambda J_0'(\lambda)}{\lambda^2 I_0(\lambda)-(1-\nu)\lambda I_0'(\lambda)}=\dfrac{\lambda^3 J_0'(\lambda)}{\lambda^3 I_0'(\lambda)}$. The coefficients B_m, C_m from Eq. (11) are to be determined numerically from the orthonormality conditions.

The angular frequencies ω_k, ω_m that correspond to the radial and flexural vibrations are:

$$\omega_k = c_L z_k = c_L\frac{\lambda_k}{a}, \tag{14}$$

$$\omega_m=\lambda_m^2\sqrt{\frac{D}{\rho h a^4}},\quad D=\frac{Eh^3}{12\left(1-\nu^2\right)}. \tag{15}$$

In all the above equations, J_0 and J_1 represent the Bessel functions of first kind and first and second order, and respectively, while I_0 and I_1 are the modified Bessel functions of first kind and first and second order.

2.2. The numerical method

The numerical model used in this paper is the finite element method, implemented in the software Comsol 4.3. A coupled field frequency analysis based on piezoelectric constitutive equations that include structural losses has been taken into consideration, for the stress-charge formulation, with the following symbol notation, according to Comsol 4.3 User Guide:

$$\begin{aligned}\sigma&=\tilde{c}_E\varepsilon-\tilde{e}^T E,\\ D&=\tilde{e}\varepsilon+\varepsilon_0\tilde{\varepsilon}_{rS}E,\end{aligned} \tag{16}$$

where σ denotes the stress matrix, ε denotes strains matrix, D denotes electric charge matrix, $\tilde{\mathbf{c}}_E$ denotes the elasticity matrix, $\tilde{s}_E$ denotes the compliance matrix, $\tilde{e}$ denotes the piezoelectric coupling matrix, $\tilde{\varepsilon}_r$ the relative permittivity matrix. In Comsol Multiphysics the $\tilde{}$ symbol denotes complex values where the imaginary part defines the dissipative function of the material: $\tilde{X} = X\left(1 \pm j\eta_X\right)$ where $\eta_X = \text{imag}\left(\tilde{X}\right)/\text{real}\left(\tilde{X}\right)$ is the loss factor.

The piezoceramic materials belong to the 6 mm class symmetry [12], and have compliance, piezoelectric coupling and relative permittivity matrices in the stress-charge form (16):

$$\mathbf{c}_E = \begin{pmatrix} c_{11} & c_{12} & c_{13} & 0 & 0 & 0 \\ & c_{11} & c_{13} & 0 & 0 & 0 \\ & & c_{33} & 0 & 0 & 0 \\ & & & c_{55} & 0 & 0 \\ & & & & c_{55} & 0 \\ & & & & & c_{66} \end{pmatrix} [\text{GPa}], \quad c_{66} = \left(c_{11} - c_{12}\right)/2, \tag{17}$$

$$\mathbf{e} = \begin{pmatrix} 0 & 0 & 0 & 0 & e_{15} & 0 \\ 0 & 0 & 0 & e_{15} & 0 & 0 \\ e_{31} & e_{31} & e_{33} & 0 & 0 & 0 \end{pmatrix} \left[\text{C/m}^2\right], \quad \boldsymbol{\varepsilon}_r = \begin{pmatrix} \varepsilon_{11} & 0 & 0 \\ 0 & \varepsilon_{11} & 0 \\ 0 & 0 & \varepsilon_{33} \end{pmatrix}.$$

2.3. Damage metrics

Damage metrics are used for damage quantification from the EMIS signature changes. Damage metrics (DM) are used to obtained the differences between the pristine and the damaged specimens.To calculate a DM value, one compares the current spectrum with a baseline spectrum (e.g., the spectrum of a pristine specimen). Commonly used DM calculations [1] are based on simple formulae that perform a point-by-point comparison of the two spectra and compute an assembly value, e.g., root mean square deviation (RMSD) and correlation coefficient deviation (CCD). RMSD and CCD are expressed in term of real part of impedance as:

$$\text{RMSD} = \sqrt{\sum_N \left[\text{Re}\left(Z_i\right) - \text{Re}\left(Z_i^0\right)\right]^2 / \sum_N \left[\text{Re}\left(Z_i^0\right)\right]^2}\,, \tag{18}$$

$$\text{CC} = \frac{1}{\sigma_Z\, \sigma_{Z^0}} \sum_N \left[\text{Re}\left(Z_i\right) - \text{Re}\left(\bar{Z}\right)\right] \times \left[\text{Re}\left(Z_i^0\right) - \text{Re}\left(\bar{Z}^0\right)\right], \quad \text{CCD} = 1 - \text{CC}\,, \tag{19}$$

where CC represents the correlation coefficient, N is the number of frequencies in the spectrum and 0 exponent represents the structure without crack. $\overline{Z}$ and $\overline{Z}^0$ denote averages and σ_Z and σ_{Z^0} represents the standard deviation.

3. RESULTS

A comparison of the analytic method and FEM computation with experimental results, at low frequemcies (10kHz–150kHz) were done in [1-4]. In this paper only analytic and FEM are done, in order to separate the effects on small geometric imperfections, or temperature effects from the study of effect intermediate and high frequencies on the EMIS method.

The geometry taken into analytical and numerical simulations are circular A2024 aluminum plate with a circular PZT-5A material for PWAS and PWAS-WL as in Figs. 2a and 2b for 2D and 3D FEM. The active sensors taken in computations are piezoelectric wafer active sensor (PWAS) and piezoelectric wafer active sensor wire lead (PWAS-WL) as in Fig. 3b, geometrical idealization of the real PWAS-WL shown in Fig. 3a.

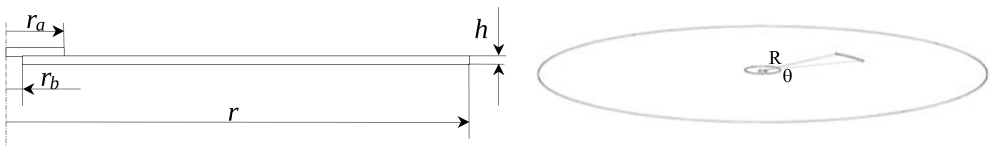

a) b)

Fig. 2 – a) Position and geometry of the thin plate with central hole in 2DFEM;
b) arc-shape laser fabricated cracks and bonded PWAS in 3D FEM.

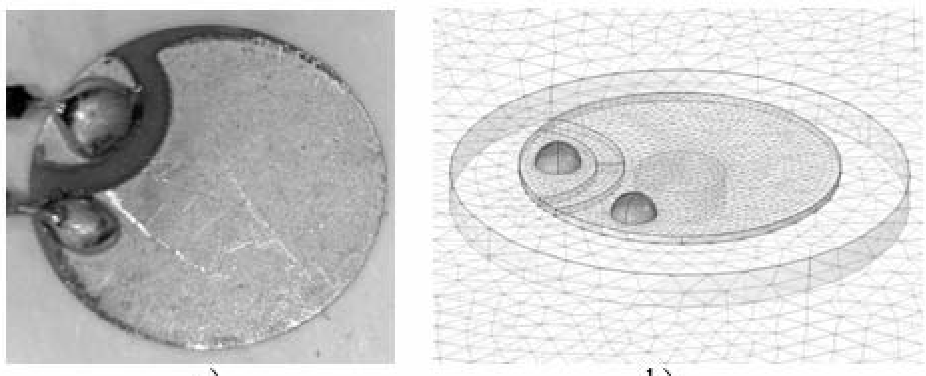

a) b)

Fig. 3 – a) Real PWAS-WL; b) ideal PWAS-WL taken in 3D FEM computations.

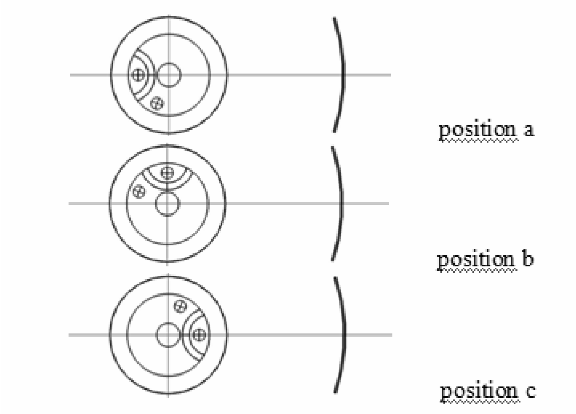

Fig. 4 – Positions of the asymmetry *versus* the crack position.

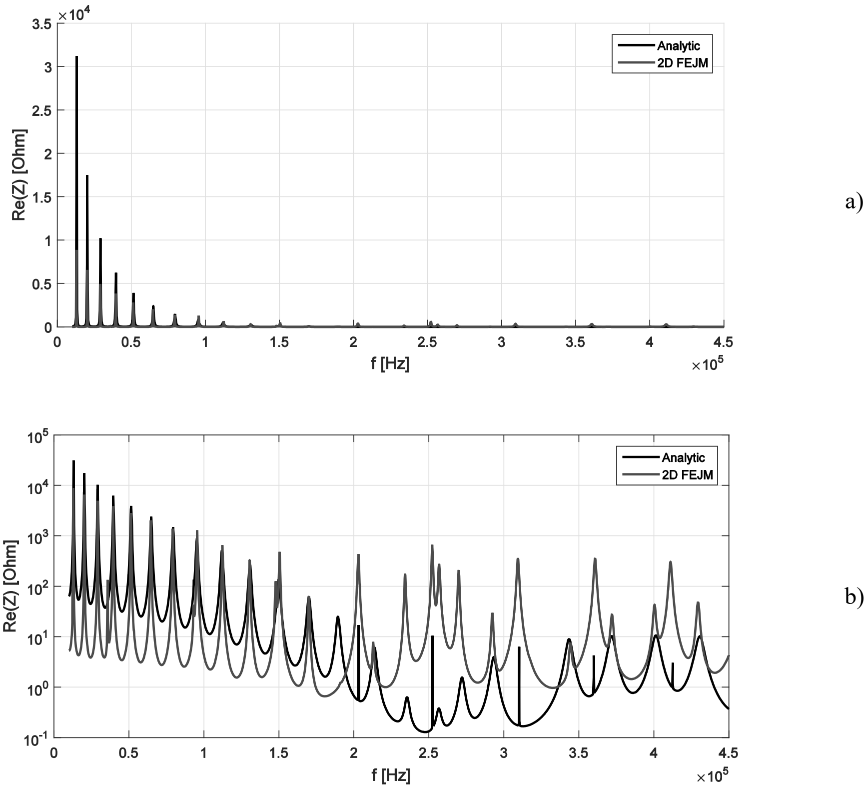

Fig. 5 – Comparisons of the analytic results with the 2D FEM numerical results from low to high frequencies; a) in linear scale: b) in logarithmic scale.

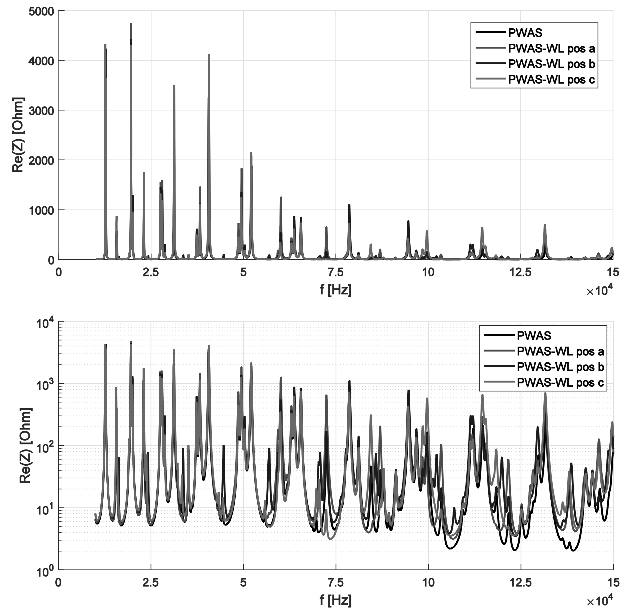

a)

b)

Fig. 6 – EMIS signature at low frequencies for the simulated crack @ 7 mm: a) in linear scale; b) in logarithmic scale.

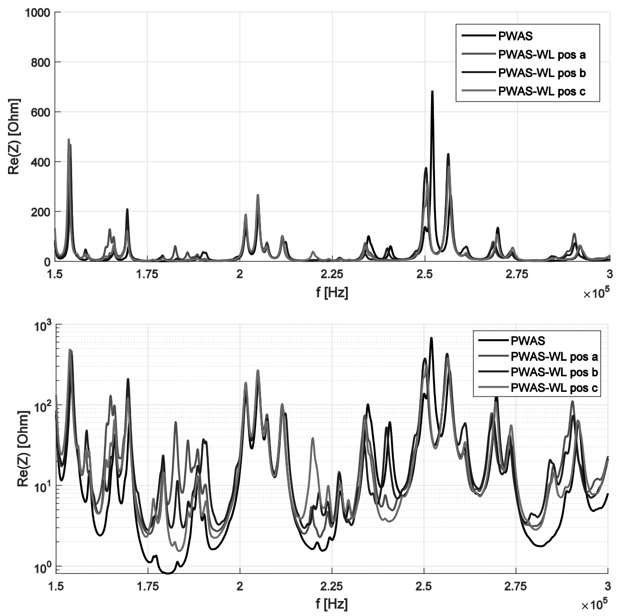

a)

b)

Fig. 7 – EMIS signature at intermediate frequencies for the simulated crack @ 7 mm: a) in linear scale; b) in logarithmic scale.

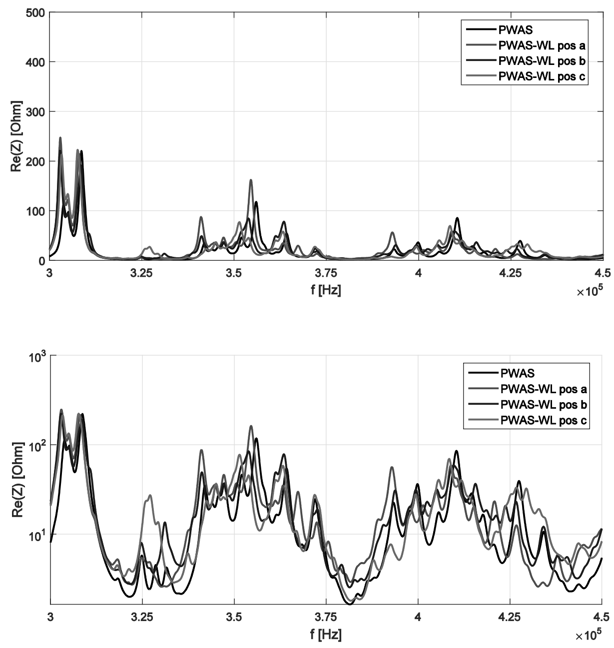

a)

b)

Fig. 8 – EMIS signature at high frequencies for the simulated crack @ 7 mm: a) in linear scale; b) in logarithmic scale.

The elastic properties of the Aluminum A2024 plate are taken $E = 70$ GPa, $\rho = 2\ 700\ \mathrm{kg/m^3}$, $\nu = 0.33$. No adhesive layer is taken into simulations as it was shown [3,4] that for a constant temperature its effect on the EMIS signature is negligible.

The piezoceramic material of the PWAS used numerical FEM computation is the piezoceramic material PZT5A, that have compliance, piezoelectric coupling and relative permittivity matrices in the stress-charge form, Eq.(16), Eq.(17): $c_{11}^E = c_{22}^E = 120.35$ GPa, $c_{12}^E = 75.18$ GPa, $c_{13}^E = c_{23}^E = 75.09$ GPa, $c_{33}^E = 110.86$ GPa, $c_{44}^E = c_{55}^E = 21.05$ GPa, $c_{66}^E = 22.57$ GPa, $e_{31} = e_{32} = -5.35116\ \mathrm{C/m^2}$, $e_{33} = 15.7835\ \mathrm{C/m^2}$, $e_{15} = 12.2947\ \mathrm{C/m^2}$, $\varepsilon_{11}^r = \varepsilon_{22}^r = 919.1$, $\varepsilon_{33}^r = 826.6$.

The specimen A2024 with bonded PWAS has the geometry (Figs.2): $r = 50.0$ mm, $h = 0.835$ mm, $r_a = 4$ mm, $r_b = 1$ mm. For 3D FEM computations, the geometries of the simulated cracks (10 mm long, 0.15 mm wide) are as follows: arc crack 1, $R = 45$ mm, $u = 13^{\circ}$; arc crack 2, $R = 25$ mm, $u = 23^{\circ}$; arc crack 3, $R = 15$ mm, $u = 38^{\circ}$; and arc crack 4, $R = 7$ mm, $u = 82^{\circ}$.

Table 1

Damage metrics at low frequencies

	pristine *vs.* crack@ 7mm	pristine *vs.* crack@ 15mm	pristine *vs.* crack@ 25mm	pristine *vs.* crack@ 45mm
	RMSD			
PWAS	1.1616	0.8259	0.6031	0.5365
PWAS-WL a	1.1567	0.7852	0.5606	0.4893
PWAS-WL b	1.1446	0.7250	0.5013	0.4358
PWAS-WL c	1.1843	0.8001	0.5804	0.5088
	CCD			
PWAS	0.9674	0.4426	0.2114	0.1622
PWAS-WL a	0.9718	0.4000	0.1788	0.1307
PWAS-WL b	0.9505	0.3287	0.1398	0.1018
PWAS-WL c	0.9831	0.4205	0.1929	0.1425

Table 2

Damage metrics at intermediate frequencies

	pristine *vs.* crack@ 7mm	pristine *vs.* crack@ 15mm	pristine *vs.* crack@ 25mm	pristine *vs.* crack@ 45mm
	RMSD			
PWAS	0.7438	0.5506	0.5890	0.4157
PWAS-WL a	0.9300	0.6542	0.6134	0.4990
PWAS-WL b	0.8838	0.6620	0.6029	0.4990
PWAS-WL c	0.8558	0.6659	0.5963	0.5100
	CCD			
PWAS	0.3374	0.1866	0.2118	0.0994
PWAS-WL a	0.5550	0.2846	0.2267	0.1484
PWAS-WL b	0.5114	0.2962	0.2164	0.1506
PWAS-WL c	0.4943	0.2992	0.2128	0.1575

Table 3

Damage metrics at high frequencies

	pristine *vs.* crack@ 7mm	pristine *vs.* crack@ 15mm	pristine *vs.* crack@ 25mm	pristine *vs.* crack@ 45mm
	RMSD			
PWAS	0.9543	0.6070	0.5254	0.2811
PWAS-WL a	0.8638	0.4363	0.3296	0.2109
PWAS-WL b	0.8167	0.4783	0.3817	0.2331
PWAS-WL c	0.8292	0.4683	0.3336	0.2028
	CCD			
PWAS	0.7152	0.2419	0.1687	0.0371
PWAS-WL a	0.6204	0.1168	0.0511	0.0184
PWAS-WL b	0.5570	0.1472	0.0776	0.0203
PWAS-WL c	0.5725	0.1393	0.0494	0.0124

First a comparison of the analytic method with 2D FEM computation of the EMIS method is done at a combined scale of low (10kHz–150kHz), intermediate (150kHz–300kHz) and high (300kHz–450kHz) frequencies. The results are shown in Fig. 5a,b in linear respectively logarithmic scale. It can be seen that at medium and high frequencies the amplitude of the EMIS signature is so small that it can be seen distinctively only in logarithmic scale, and the analytic results are in a reasonable agreement with the 2D FEM numerical ones.

Comparisons of the effect of the asymmetry of the PWAS-WL with respect to the crack position involved in this SHM method at low, medium and high frequencies are shown in Fig. 6, Fig. 7 and Fig. 8 for the simulated crack at 7 mm. It can be seen that at low frequencies in logarithmic scale the differences between the normal PWAS and the PWAS-WL (any position) are small, while at medium and high frequencies the differences are bigger. This can be seen also in the DM Tables 1, 2, 3 in RMSD and CCD coefficients for the simulated crack at 7 mm. It is related to the wavelength of the standing wave compared with the PWAS and PWAS-WL dimensions, and particularly with the PWAS-WL active part.

It was shown both experimentally and numerically in [1-3]. that for low frequencies DM has the ability to works well for the quantification of the distance to the crack. However, numerically, at medium and high frequencies, ~~at~~ it can be seen in Table 1, Table 2 and Table 3, that only crack at $7\,\mathrm{mm}$ has distinct DM values, while cracks at $15\,\mathrm{mm}$, $25\,\mathrm{mm}$ and $45\,\mathrm{mm}$ have weak DM differences. For example at low frequencies the RMSD DM on a PWAS-WL(a) for cracks at $7\,\mathrm{mm}$, $15\,\mathrm{mm}$, $25\,\mathrm{mm}$, $45\,\mathrm{mm}$ are 1.1567, 0.7852, 0.5606, 0.4893. The differences between these DM are big enough to distinguish between the cracks at any distances, despite the small numerical errors that can occur. At intermediate and high frequencies the RMSD DM on a PWAS-WL(a) for cracks at $7\,\mathrm{mm}$, $15\,\mathrm{mm}$, $25\,\mathrm{mm}$, $45\,\mathrm{mm}$ are 0.9300, 0.6542, 0.6134, 0.4990 respectively 0.8638, 0.4363, 0.3296, 0.2109. At intermediate and high frequencies only the difference between the firsts DM values and the others are big enough to distinguish a crack at $7\,\mathrm{mm}$ from the others. The other values show weak differences that mixed with numerical errors may not distinctively determine the distance to the crack. Combined with other geometrical small imperfections, described in [3], experimentally the DM may work only for cracks in the close vicinity of the PWAS and PWAS-WL for intermediate and high frequencies.

4. CONCLUSIONS

From the theoretical point of view the analytic method that predicts the EMIS signature is in acceptable agreement with the numerical 2D FEM computations, even at intermediate and high frequencies.

From the theoretical 3D FEM point of view the EMIS method work well, based on DM, both RMSD and CCD, for the low frequencies spectrum, and acceptable for intermediate and high frequencies for cracks in the close vicinity of the PWAS.

Instead, for cracks away from the PWAS the EMIS method barely works acceptable for intermediate and high frequencies only theoretically.

Combined with small geometrical imperfections and small temperature variations, experimentally the EMIS method on intermediate and high frequencies spectrum may work only for cracks in the close vicinity of the PWAS.

Received on May 13, 2019

REFERENCES

1. GIURGIUTIU, V., *Structural health monitoring with piezoelectric wafer active sensors*, Elsevier Academic Press, Second edition, 2014.
2. ZAGRAI, A., GIURGIUTIU, V., *Electro-mechanical impedance method for crack detection in thin plates*, Journal of Intelligent Material Systems and Structures, **12**, *10*, pp. 709–718, 2001.
3. RUGINA, C., ENCIU, D., TUDOSE, M., *Numerical and experimental study of circular disc electromechanical impedance spectroscopy signature changes due to structural damage and sensor degradation*, Structural Health Monitoring, **14**, *6*, pp. 663–681, 2015.
4. RUGINA, C., TOADER, A., GIURGIUTIU, V., URSU, I., *The electromechanical impedance method for structural health monitoring of thin circular plates*, Proceedings of the Romanian Academy – Series A, **15**, *3*, pp. 272–282, 2014.
5. ENCIU, D., URSU, I., TOADER, A., *New results concerning structural health monitoring technology qualification for transfer to space vehicles,* Structural Control and Health Monitoring, **24**, *10*, p. e1992, 2017; DOI 10.1002/stc.1992.
6. KAMAS, T., GIURGIUTIU, V., LIN, B., *E/M impedance modeling and experimentation for the piezoelectric wafer active sensor*, Smart Materials and Structures, **24**, *11*, pp. 5040–5053, 2015.
7. NA, W.S., BAEK, J., *A review of the piezoelectric electromechanical impedance based structural health monitoring technique for engineering structures*, Sensor, **18**, *5*, p. 1307, 2018**,** DOI:10.3390/s18051307.
8. CAMPEIRO, L.M., DA SILVEIRA, R.Z.M., BAPTISTA F.G., *Impedance-based damage detection under noise and vibration effects*, Structural Health Monitoring, **17**, *3*, pp. 654–667, 2017.
9. GIANESINI, B.M., CORTEZ, N.E., ROTHSCHILD, A.A., FILHO J.V., *Modeling, simulation and analysis of temperature effects oniImpedance-based SHM applications using Finite Elements*, Structural Health Monitoring 2017; The 11th International Workshop on Structural Health Monitoring, IWSHM 2017; DOI: 10.12783/shm2017/13916.
10. TOADER, A., URSU, I., ENCIU, D., *New Advances in Space SHM Project*, INCAS Bulletin, **7**, *1*, pp. 65–80, 2015.
11. URSU, I., GIURGIUTIU, V., TOADER, A., *Towards spacecraft applications of structural health monitoring*, INCAS Bulletin, **4**, *4*, pp. 111–124, 2012.
12. *** IEEE std 176-1987 – *Standard on Piezoelectricity*, DOI: 10.1109/IEEESTD.1988.79638.